Petroleum Science 20 (2023) 1446–1457

Contents lists available at ScienceDirect

Petroleum Science

journal homepage: www.keaipublishing.com/en/journals/petroleum-science

Original Paper

# Fractionation characteristics of magnesium isotope in the ancient weathering crust

Jia-Qi Yang [a, b], Jun-Tao Zhang [b, d], Zhi-Liang He [c, *], Ni-Na Luo [e], Xiao-Hui Jin [b, d], Tao Zhang [b, d], Ning Gu [b, d], Kang-Jun Huang [f], Jian Gao [b, d]

[a] School of Energy Resources, China University of Geosciences, Beijing, 100083, China
[b] SINOPEC Exploration and Production Research Institute, Beijing, 100083, China
[c] China Petrochemical Corporation Ltd., Beijing, 100728, China
[d] Key Laboratory of Deep Geology and Resources, SINOPEC, Beijing, 102206, China
[e] Chongqing Gas Field of PetroChina Southwest Oil and Gas Field Company, Chongqing, 400021, China
[f] Shaanxi Key Laboratory of Early Life and Environments, Department of Geology, Northwest University, Xi'an, Shaanxi, 710069, China

ARTICLE INFO

*Article history:*
Received 14 February 2022
Received in revised form
31 August 2022
Accepted 29 December 2022
Available online 30 December 2022

Edied by Jie Hao and Teng Zhu

*Keywords:*
Magnesium isotope
Dolomitization mode
Weathering
Ancient weathering crust
Ordos Basin

ABSTRACT

Weathering has always been a concerned around the world, as the first and most important step in the global cycle of elements, which leads to the fractionation of isotopes on the scale of geological age. The Middle Ordovician Majiagou Formation in Daniudi area of the Ordos Basin had experienced weathering for >130 Myr. Through thin section observation, major and trace element analysis, carbon, oxygen, and magnesium isotopes composition analysis, the dolomitization modes and weathering of ancient dolomite in Daniudi area were analyzed in detail. The results showed that the Sabkha and brine-reflux dolomitization modes had developed, and the Mg isotopes in different layers of the karst crust were fractionated by various factors. The vertical vadose zone was affected by weathering, the Mg isotope of dolomite ($\delta^{26}Mg_{dol}$) showed a downward decreasing trend; the horizontal underflow zone was controlled by diagenesis and formation fluid, $\delta^{26}Mg_{dol}$ showed a vertical invariance and negative; the main reason for Mg isotope fractionation in the deep slow-flow zone was the brine-reflux dolomitization mode during early burial period, which showed a vertical downward increase. Finally, the Mg isotope characteristic data of the ancient weathering crust were provided and the process of Mg isotope fractionation in the karst crust was explained.


## 1. Introduction

Magnesium isotope exhibits significant fractionation during weathering and the intensity is much stronger at low temperatures (Li et al., 2015; Guo et al., 2019). The weathering of carbonate rocks can lead to the depletion of the $^{24}Mg$ isotope, eventually the compositions of the $^{26}Mg$ isotope ($\delta^{26}Mg$) reaching +1.8‰ (Oskierski et al., 2019), and is relatively large compared to the differentiation process of magma which can be observed (Teng et al., 2016). Therefore, the Mg isotope has the potential to characterize low-temperature geochemical processes.

With the rise and development of high-precision Mg isotope testing technology (Galy and France-Lanord, 2001; Ke et al., 2011; Gao et al., 2016), Mg isotope has gradually become an essential geochemical proxy for the study of dolomite (Azmy et al., 2013; Mavromatis et al., 2014; Geske et al., 2015a). Many researchers have targeted the fractionation of Mg isotope to systematically analyze the impact of weathering (Pokrovsky et al., 2011; Li et al., 2020; Chen et al., 2020), and dolomitization (Bialik et al., 2018; Ning et al., 2020; He R. et al., 2020). The correlation between the Mg/Al ratio and $\delta^{26}Mg$ of the Doushantuo cap dolomite indicated that it was formed by weathering and had a lower strength than the Nantuo Formation (Li et al., 2020). The granite from the eastern Peninsular Ranges Batholith preserved the chemical weathering signal in the form of O and Mg isotopes, and $\delta^{26}Mg$ from −0.404 to +0.441‰ suggested that the low Mg content of the Upper Continental crust in the Phanerozoic might not be caused by the hierarchical crystallization of igneous rocks (Shen et al., 2009). Although Mg isotope

* Corresponding author.
*E-mail address:* hezhiliang@sinopec.com (Z.-L. He).

https://doi.org/10.1016/j.petsci.2022.12.014

in rivers showed significant fractionation during weathering (Tipper et al., 2012), glacial weathering had little effect on continental runoff (Wimpenny et al., 2011). Mg isotope has been widely used in weathering processes, however, there are few reports on carbonate weathering formation, especially in ancient formations.

The fractionation of Mg isotope is affected by many factors, such as temperature (Li et al., 2015), the form of Mg in an aqueous solution (Schott et al., 2016), and the types of minerals formed (Wang et al., 2013). And Mg isotope fractionation occurs in different reservoirs (Fig. 1). $\delta^{26}$Mg of rivers and groundwater are controlled by rock type, secondary mineral formation, and biological incorporation (Wimpenny et al., 2011). In large rivers, the Mg abundance and isotopic composition of water appear to be dominated by weathering reactions (Tipper et al., 2012). The rate of mineral dissolution controls the release of Mg from the primary phase, while the nature of the phase formed determines the ability to incorporate secondary minerals. For example, heavy Mg isotope preferentially enters the secondary montmorillonite (Tipper et al., 2006), and isotopic fractionation is attributed to the formation of secondary clay minerals preferentially utilizing $^{26}$Mg. In contrast, calcium carbonate preferentially incorporates light Mg isotope, and heavy isotope remains in residual water (Gao et al., 2016). The importance

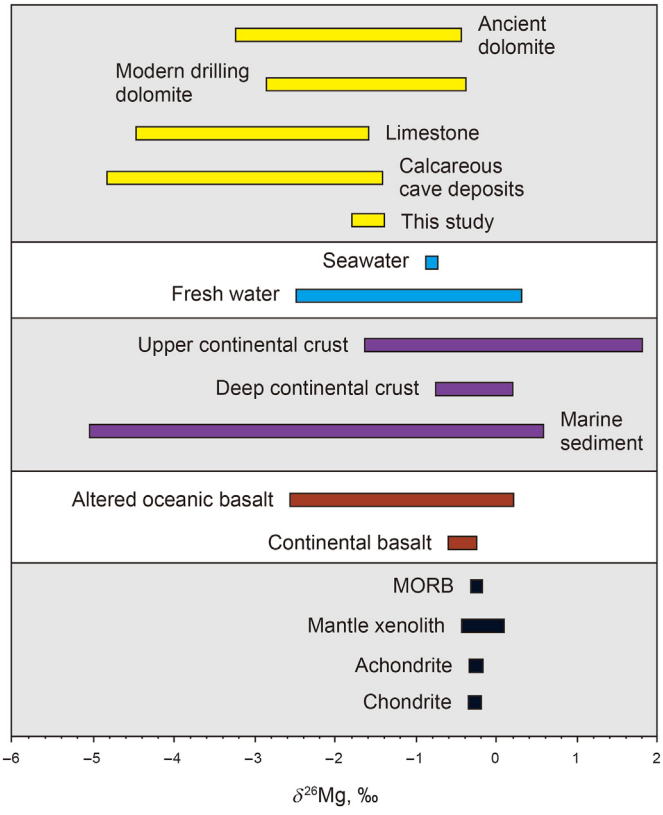


**Fig. 1.** Mg isotopic distribution in major meteorite and terrestrial reservoirs. $\delta^{26}$Mg of seawater (Foster et al., 2010; Ling et al., 2011), fresh water (Mavromatis et al., 2014; Ma et al., 2015; Dessert et al., 2015), ancient dolomite (Lavoie et al., 2014; Geske et al., 2015a; Peng et al., 2016), modern drilling dolomite (Blattler et al., 2015; Higgins and Schrag, 2010), limestone (Immenhauser et al., 2010; Kasemann et al., 2014; Galy et al., 2002), calcareous vug deposits (Galy et al., 2002; Immenhauser et al., 2010), upper continental crust (Li et al., 2010; Ke et al., 2016), deep continental crust (Teng et al., 2013; Wang et al., 2015), marine sediment (Higgins and Schrag, 2010; Geske et al., 2015b), altered oceanic basalt (Yang et al., 2012; Huang J. et al., 2015), mid-ocean ridge basalts (MORB) (Teng et al., 2016; Bourdon et al., 2010), mantle xenolith (Pogge von Strandmann et al., 2011; Hu et al., 2016; Wang et al., 2016) achondrite (Chakrabarti and Jacobsen, 2010; Sedaghatpour and Teng, 2016) and chondrite (Schiller et al., 2010; Pogge von Strandmann et al., 2011) have different distribution ranges.

of rock type is evident in smaller monolithic catchments, where carbonate-dominated catchments typically produce water with a lighter Mg isotopic composition than silicate-dominated catchments (Tipper et al., 2012). The sharp drop in $\delta^{26}$Mg near the top of the Nantuo Formation indicated a decrease in weathering intensity which might have extended to the interval during caprock carbonate deposition, and the low weathering intensity was attributed to the decrease in atmospheric $pCO_2$ (Li et al., 2020).

The influence of different factors on the $\delta^{26}$Mg must be carefully considered when using the Mg isotope for analysis. The meaning of a single $\delta^{26}$Mg value may not be clear; however, the variation trend might represent the fractionation process in certain chemical processes (Ning et al., 2020). This study, therefore, focuses on the influence of various factors on geochemical signals during the period of uplift, and specific dolomitization and/or weathering processes represented by the variation trend of the Mg isotope compositions of dolomite ($\delta^{26}Mg_{dol}$) (e.g., Tipper et al., 2012; Li et al., 2015).

The Majiagou Formation of the Middle Ordovician in the Ordos Basin experienced a long period of weathering. To further improve the fractionation mechanism of Mg isotope and assess the weathering, we have taken the Majiagou Formation as an example to systematically study the influence of weathering on the ancient dolomite and explore the fractionation state of Mg isotope after being affected by weathering. We also discuss and analyze (1) the dolomitization modes in the evaporitic tidal flat environment; (2) the control of dolomitization modes on Mg isotope fractionation; (3) the influence of weathering on the fractionation of Mg isotope in different layers; (4) and we provide a new process of isotope evolution under the interaction of dolomitization and weathering.

## 2. Geological backgrounds

The Ordos Basin, the second largest sedimentary basin in China, is located in the western part of the North China Platform, with a total area of about 37 × $10^4$ km$^2$ (Su et al., 2012; Xie et al., 2020; Sun, 2020). The basin can be divided into six structural units: the Yimeng uplift, the Weibei uplift, the Jinxi fault-fold belt, the Yishan slope, the Tianhuan syncline, and the fault-fold belt of the western margin; the Daniudi area is located in the northeast of the Yishan slope (Fig. 2). The Majiagou Formation mainly consists of carbonate rocks that were deposited in the main part of the Ordos Basin during the Middle Ordovician.

There are three transgressions (2nd, 4th, and 6th members of Majiagou Formation, Ma2, Ma4, and Ma6) and three regressions (Ma1, Ma3, and Ma5), and the Ma1, Ma3, and Ma5 Members are mainly dolomite, gypsum and salt rock with a small amount of limestone, the Ma2, Ma4, and Ma6 Members are limestone and dolomite (Yang, 2011; He et al., 2013; Xi et al., 2017). The Ma5 Member can be further divided into 10 sub-members longitudinally (Jia and Ding, 2016; Xie et al., 2020), $Ma5_{10}$ to $Ma5_1$ are deposited from bottom to top. And the main stratum in this study is the upper part of the Ma5, which is mainly composed of dolomite and limestone (Fig. 3). There is obvious zoning in the vertical direction, the $Ma5_5$ is in the stage of rising sea level, and mainly deposits a set of pure dolomite and limestone; the $Ma5_{3+4}$ are at the lowest point of a smaller regression cycle, deposited dolomite interbedded with gypsum rock, with the highest gypsum content; while the $Ma5_{1+2}$ are in the stage of regression, a gypsum-bearing dolomite stratum was deposited (Yang, 2011; Yang et al., 2022).

After the Middle Ordovician, affected by the Caledonian Movement, the whole basin was uplifted, then experienced weathering for up to 130 Myr (Yang, 2011; Jia and Ding, 2016). The widely distributed bauxite above $Ma5_{1+2}$ was discovered, which is direct evidence of long-term weathering in the study area (e.g., He et al., 2013; Jia and Ding, 2016). The thick dolomite developed in the

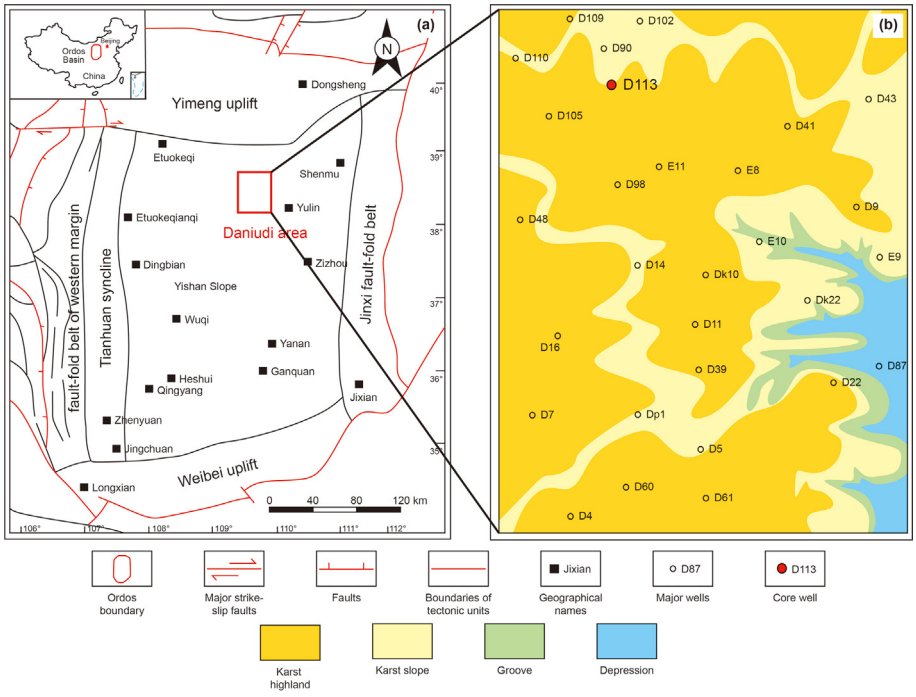


**Fig. 2.** Map showing the structural location (a) and the drilling wells of the Daniudi area (b) in the Ordos Basin.

evaporitic tidal flat environment of the Middle Ordovician was seriously affected by weathering (Zhang et al., 2016; He Z. et al., 2020).

## 3. Methods

All 29 samples are from well D113, located at the karst slope, which is the drilling that coring the entire $Ma5_{1-5}$ section. For comparative study using petrographic, mineralogical characteristics, elemental, carbon, oxygen, and magnesium isotopic analyses. The micropetrography observations were carried out in the SINOPEC's Key Laboratory for Petroleum Reservoir.

The concentrations of major elements were measured by PerkinElmer 5300DV ICP–OES at the Analytical Laboratory of Beijing Research Institute of Uranium Geology (ALBRIUG), using 6 powder samples, digested in a mixture of ultra-high purity $HNO_3 + HCl + HF$ in high-pressure Teflon cups, as described by Gao et al. (2015). Trace elements were determined by PerkinElmer NexIon300D ICP–MS using sample powders digested according to the above method.

Stable carbon and oxygen isotopic composition of the carbonate powder of the 10 samples were measured in the ALBRIUG using a Finnegan MAT253 mass spectrometer and using the phosphoric acid treatment method reported by the authors (Zhao et al., 2016; Lash, 2018; Zhang et al., 2022). The values of $\delta^{13}C$ and $\delta^{18}O$ are reported in δ per unit (‰) relative to the Vienna–Pee·Dee·Belemnite (V–PDB) standard and the Vienna Standard Mean Ocean Water (V–SMOW), respectively.

Mg isotope was measured in the International Key Laboratory of Continental Dynamics, Northwest University, China. 8 samples were ground into 50 mg powder in a pre-cleaned agate mortar, then placed in a Teflon beaker and dissolved in 5 mL 4.2N $HNO_3$ as the stock solution. Two ion exchange columns were used to recover the Mg in each sample, which was described in detail by Hu et al. (2017). A 1 ppm Mg-solution in 2% $HNO_3$ was measured using a Thermo Fisher Scientific Neptune Plus MC–ICP–MS. The instrument operates with a medium-mass-resolution mode, using a 100 mL/min self-priming nebulizer and a dual-channel glass spray chamber. Standard-sample bracketing was used for quality deviation correction. The sample concentration is usually combined with the internal standard and is better than ±10%. The typical internal accuracy (2 standard errors or 2 SE) of $^{26}Mg/^{24}Mg$ is better than ±0.04‰, and $^{25}Mg/^{24}Mg$ is better than ±0.02‰. Based on repeat analyses of multiple Mg standard solutions, the long-term external reproducibility is better than ±0.1‰. The pure Mg solutions of Cambridge1 and DSM3 were used to monitor the accuracy of Mg isotope analysis. All test data are standardized according to the international Mg isotope standard, using the traditional δ notation to indicate deviations per thousand. $\delta^{26}Mg$ and $\delta^{25}Mg$ are calculated relative to the standard DSM3:

$$\delta^x Mg = \left[ \left( \delta^x Mg / \delta^{24} Mg \right)_{sample} \Big/ \left( \delta^x Mg / \delta^{24} Mg \right)_{DMS3} - 1 \right] \times 1000$$

where $x$ refers to mass 25 or 26. In order to verify the accuracy of the chemical procedures, IAPSO seawater standard samples and USGS rock standard samples are processed together with the samples in the ion exchange program.

## 4. Results

### 4.1. Petrological characteristics

Three major rock types were found in Majiagou Formation according to the criteria established by Sibley and Gregg (1987): gray-micrite dolomite which can be further divided into micrite dolomite with gypsum mold pore (RD1) and micrite dolomite with breccia (RD2), dark gray-silty dolomite (RD3) and dark gray-silty limestone (L1), while different rock types are concentrated in different strata (Fig. 3).

RD1 mainly developed in the $Ma5_{1+2}$. Near longitudinal solution

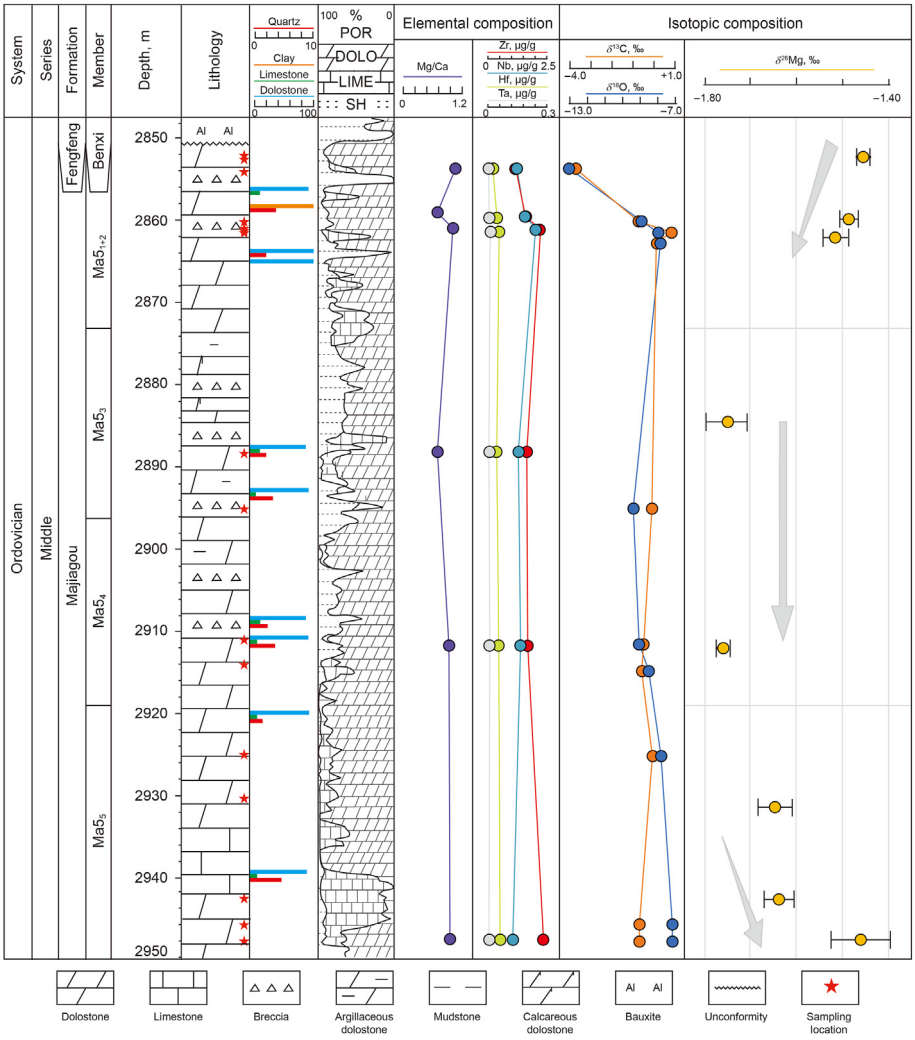


**Fig. 3.** Lithologic histogram and elements, isotopes composition distribution of well D113 (There are three isotopic variation trends developed in the Ma5 member, and a certain correlation between Mg isotope and C/O isotopes in the longitudinal section).

fractures, small-scale karst vugs, and argillaceous nodules developed in this part could be observed on core samples (Fig. 4a–c). The fractures are filled by residual materials such as infiltrated aluminous mudstone (Fig. 4b). Under the microscope, the dolomite crystal size of this type is shown in Fig. 4g and h, is the smallest in the study area, mainly less than 5 μm. A large number of gypsum mold pores can be observed, and some of them were semi-filled with dolomite and/or little later ankerite whose grain size is larger and crystal form is complete, most mold pore shapes are mainly round and rectangular.

RD2 mainly developed in the $Ma5_{3+4}$. The core is characterized by network or near horizontal dissolution fractures and colluvial breccia (Fig. 4d and e). The size of matrix dolomite is less than 5 μm, however, the volume of cement is large. Secondary calcite and dolomite cements in large numbers could be observed in the dissolution pores due to late cementation (Fig. 4i and j).

RD3 and L1 are the main rock types in the $Ma5_5$. The size of the matrix in this part is obviously larger than that of the upper, which is silty, approximately 20–30 μm. Dolomite developed in the upper part (Fig. 4k and l) and limestone in the lower part (Fig. 4f); and the upper part RD3 with a few fractures can be observed, are important storage space (Fig. 4l).

### 4.2. Isotopic characteristics

The obtained C and O isotopes showed large fractionation results, with the C isotopes ranging from −3.8‰ to +0.8‰, and the O isotopes are −13.1 to −7.2‰ (Fig. 3). In the $Ma5_{3-5}$, the $\delta^{13}C$ content showed a slow upward trend, from the lowest $\delta^{13}C$ content in the $Ma5_5$ about −0.7‰ to the +0.8‰ at the top of the $Ma5_{3+4}$. There is no obvious correlation between the C/O isotopes of the $Ma5_{3-5}$ (Fig. 5). However, in the $Ma5_{1+2}$, the C isotopes of these strata appear to be significantly negatively biased. The closer the overlying bauxite is, the more negative the $\delta^{13}C$ content is, until the $\delta^{13}C$ content of the top surface of the $Ma5_{1+2}$ can be reached −3.8‰ (Fig. 3). And the C/O isotopes showed an obvious correlation in these strata (Fig. 5).

Mg isotopic composition in the study area is tabulated in Table 1, $\delta^{26}Mg_{dol}$ and $\delta^{25}Mg_{dol}$ crossplot is shown in Fig. 6. The $\delta^{26}Mg_{dol}$ ranges −1.75 to −1.47‰, and the $\delta^{25}Mg_{dol}$ ranges −0.91 to −0.75‰. Mg isotope showed an excellent correlation between the obtained samples and standard samples in a scatter diagram, indicating that the measured Mg isotope composition data are truly available. There are obvious differences between the $\delta^{26}Mg_{dol}$ of different strata. The average $\delta^{26}Mg_{dol}$ of the $Ma5_{1+2}$ is −1.63‰. The $\delta^{26}Mg_{dol}$

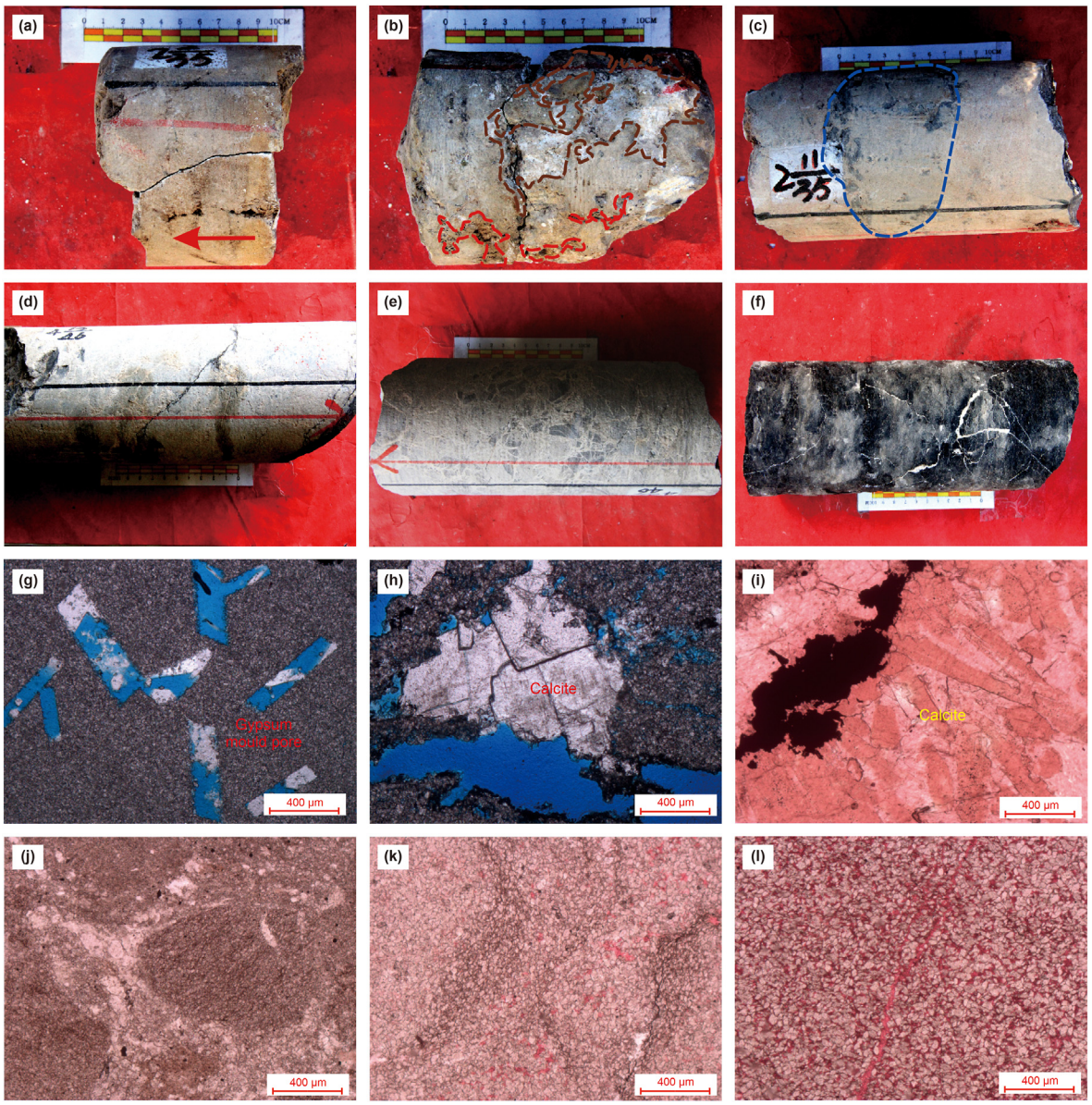


**Fig. 4.** Carbonate rocks developed in the Ma5 Formation in the D113 well. (a) Gray argillaceous dolomite with longitudinal solution fractures, 2–4/35, 2855 m, $Ma5_{1+2}$; (b) Gray argillaceous dolomite, vug is filled with mud, and residual longitudinal solution fractures, 2–5/35, 2855.1 m, $Ma5_{1+2}$; (c) Gray argillaceous dolomite with argillaceous nodule, 2–11/35, 2856.2 m, $Ma5_{1+2}$; (d) Dark gray-micritic dolomite, network solution fractures filled with calcite, 4–13/46, 2871.67 m, $Ma5_{3+4}$; (e) Dark gray-breccia dolomite, solution fractures filled with calcite, 4–14/46, 2871.75 m, $Ma5_{3+4}$; (f) Dark gray-silty limestone, cracks are filled with calcite, 10–51/54, 2930 m, $Ma5_5$; (g) Gypsum mold pores are developed in micritic dolomite, D113–22, 2862.21 m, $Ma5_{1+2}$, plane-polarized light (PPL); (h) Breccia, gypsum mold pores filled with ferrodolomite, D113–25, 2861.71 m, $Ma5_{1+2}$, PPL; (i) Fracture filling secondary calcite cement, D113–20, 2887.75 m, $Ma5_3$, PPL; (j) Breccia, filled with argillaceous dolomite, D113–15, 2902.57 m, $Ma5_4$, PPL; (k) Mud bearing silty dolomite, D113-5, 2934.91 m, $Ma5_5$, PPL; (l) Calcareous dolomite, D113-7, 2931.01 m, $Ma5_5$, PPL. The red arrow is the longitudinal dissolution pores, the red dotted line is the dissolution pore, the brown line is the vug filling bauxite, and the blue line is the argillaceous nodule.

of the $Ma5_{3+4}$ is negative, and the average is −1.75‰, while the average $\delta^{26}Mg_{dol}$ in the $Ma5_5$ is −1.49‰ (Fig. 7). In addition, we measured the $\delta^{26}Mg$ of the dissolved residual silica in some samples, which are significantly higher than that in the matrix, from −0.6‰ to +0.6‰ (Table 1).

There is a strong correlation between $\delta^{26}Mg_{dol}$ with $\delta^{13}C$ and $\delta^{18}O$ (Fig. 8). In the $Ma5_{1+2}$, $\delta^{26}Mg_{dol}$ gradually decreases with the increase of the $\delta^{13}C$ and $\delta^{18}O$. However, due to the relatively small amount of data in other layers, we cannot directly observe the corresponding coupling changes.

### 4.3. Elements characteristics

The experiment measured the trace elements and major elements of 6 samples, and the specific data is shown in Table 2. The content of CaO is mainly distributed between 29.7%–34.58%, and MgO is distributed between 17.06%–22.27%. There is no significant change in major elements including Na, Al, and Ti, and the contents of CaO and MgO in most samples are similar, but a few samples have high calcite content which produced higher content of CaO. In addition, the quartz content of some samples is high, which made it

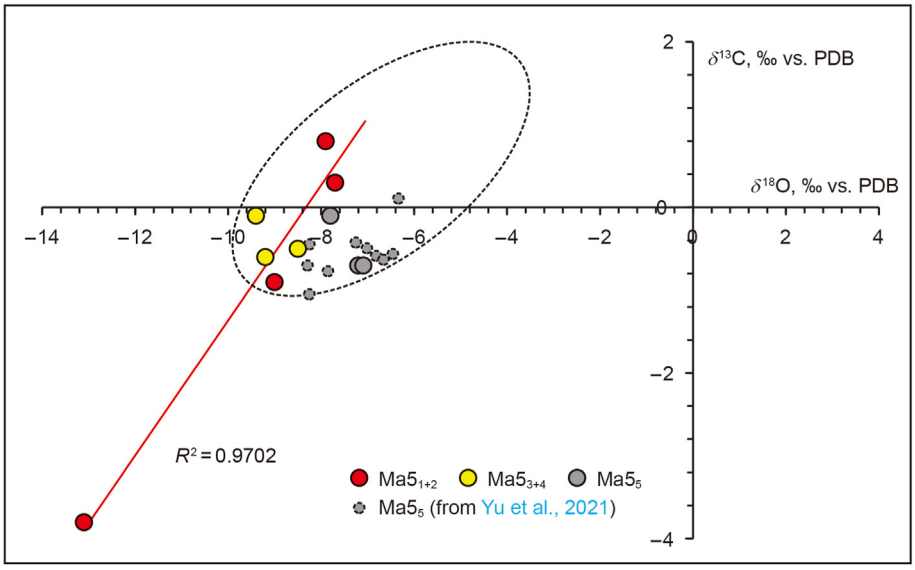


**Fig. 5.** The distribution of C/O isotopes in different subsegments in the study area. There is an obvious correlation between the $Ma5_{1+2}$ formations, but there is no correlation between the $Ma5_{3+4}$ and $Ma5_5$. The dotted line shows the distribution range of C/O isotopes of the Middle Ordovician carbonate samples around the world, and the straight line shows the correlation of C/O isotopes of the $Ma5_{1+2}$ sub-members in Daniudi area. The data of the small gray circle comes from Yu et al. (2021).

**Table 1**
Mg and C/O isotopic compositions of dolomite near weathering crust in the Daniudi area of the Ordos Basin.

| Type | Sample | Depth, m | Formation | C/O isotopic compositions, ‰ | | | Mg isotopic compositions, ‰ | | | | Components |
|---|---|---|---|---|---|---|---|---|---|---|---|
| | | | | $\delta^{13}C_{V-PDB}$ | $\delta^{18}O_{V-PDB}$ | $\delta^{18}O_{V-SMOW}$ | $\delta^{25}Mg$ | 2SD | $\delta^{26}Mg$ | 2SD | |
| Standard | Alfa Mg | | | | | | −2.00 | 0.06 | −3.92 | 0.11 | |
| | BHVO−2 | | | | | | −0.09 | 0.07 | −0.28 | 0.14 | |
| | Seawater | | | | | | −0.44 | 0.04 | −0.85 | 0.07 | |
| Sample | D113−1 | 2948.03 | $Ma5_5$ | −0.7 | −7.2 | 23.4 | −0.83 | 0.01 | −1.61 | 0.04 | Carbonate |
| | D113−1* | 2948.03 | | / | / | / | 0.01 | 0.02 | +0.06 | 0.04 | Silicate |
| | D113−2 | 2946.01 | | −0.7 | −7.2 | 23.5 | / | / | / | / | Carbonate |
| | D113−3 | 2943.07 | | / | / | / | −0.85 | 0.02 | −1.64 | 0.05 | Carbonate |
| | D113−3* | 2943.07 | | / | / | / | −0.03 | 0.03 | −0.06 | 0.03 | Silicate |
| | D113−7 | 2931.01 | | / | / | / | −0.81 | 0.09 | −1.64 | 0.06 | Carbonate |
| | D113−9 | 2925.51 | | −0.1 | −7.8 | 22.9 | / | / | / | / | Carbonate |
| | D113−12 | 2914.76 | $Ma5_{3+4}$ | −0.5 | −8.5 | 22.1 | / | / | / | / | Carbonate |
| | D113−13 | 2911.9 | | −0.6 | −9.2 | 21.4 | −0.91 | 0.04 | −1.74 | 0.01 | Carbonate |
| | D113−17 | 2895.97 | | −0.1 | −9.4 | 21.2 | / | / | / | / | Carbonate |
| | D113−21 | 2888.75 | | / | / | / | −0.89 | 0.07 | −1.75 | 0.07 | Carbonate |
| | D113−22 | 2862.21 | $Ma5_{1+2}$ | +0.3 | −7.7 | 23 | / | / | / | / | Carbonate |
| | D113−25 | 2861.71 | | +0.8 | −7.9 | 22.7 | −0.80 | 0.02 | −1.51 | 0.06 | Carbonate |
| | D113−28 | 2860.3 | | −0.9 | −9 | 21.6 | −0.76 | 0.03 | −1.49 | 0.03 | Carbonate |
| | D113−29 | 2854.04 | | −3.8 | −13.1 | 17.4 | −0.75 | 0.05 | −1.47 | 0.02 | Carbonate |

impossible to judge the weathering intensity according to the Si content. And the content of Fe, MnO, and Sr is low (Tables 2 and 3).

There is a certain correlation between weathering and mineral trace elements. As shown in Fig. 9, the trace element composition of the samples in the study area changed with the degree of weathering. Among them, the correlation between Zr−Hf is well, and there is also a certain correlation between Nb−Ta.

## 5. Discussions

### 5.1. Dolomitization process

#### 5.1.1. Sabkha dolomitization mode

RD1 and RD2 were developed by Sabkha dolomitization mode during the penecontemporaneous period (Jia and Ding, 2016; Zhang et al., 2017; Sun, 2020). Petrological characteristics, the small size of the micritic dolomite and gypsum during the sedimentary period which was dissolved to form gypsum mold pore in RD1 (Fig. 4g and h) and breccia in RD2 (Fig. 4i and j), indicate RD1 and RD2 are developed in the Sabkha dolomitization (Allan and Wiggins, 1993; Warren, 2000). Affected by the evaporitic tidal flat environment, during $Ma5_{1+2}$, large-scale gypsum-bearing dolomite could easily be developed by the dolomitization process after the deposition of primary aragonite and calcite. And the sea level was at the lowest point of a transgressive-regression system in the $Ma5_{3+4}$ period, therefore, the scale of sedimentary gypsum is larger than that of $Ma5_{1+2}$ forming gypsum formations.

The major elements and Sr characteristics of different layers are similar (Table 2). The $\delta^{13}C$ content of the top surface of the $Ma5_{1+2}$ can reach −3.8‰, and the correlation of C/O isotopes is very high ($R^2$ = 0.97) (Figs. 3 and 5). Bauxite, as one of the products of weathering, proves that weathering could be a key factor to cause

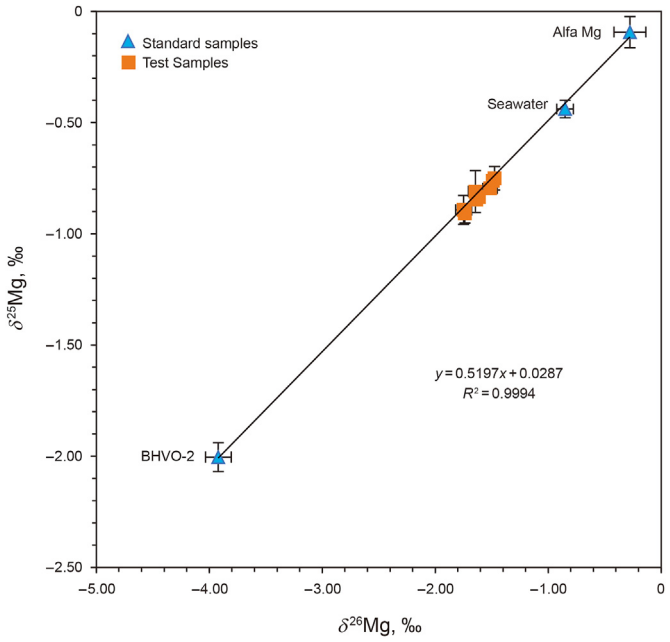


**Fig. 6.** Mg isotope crossplot of the samples and standards.

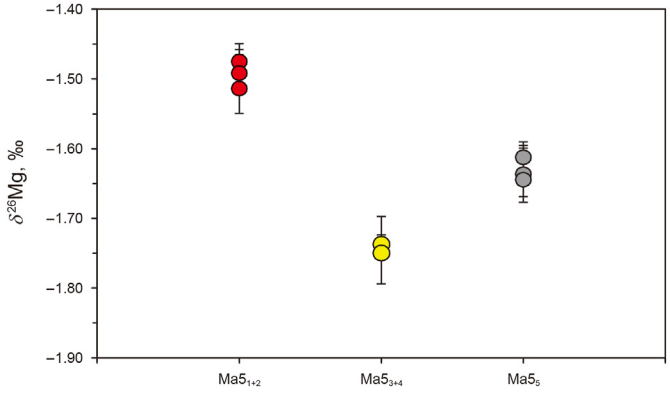


**Fig. 7.** There are obvious differences in $\delta^{26}Mg_{dol}$ in different layers (The legend is shown in Fig. 5).

this phenomenon is possible, resulting in C/O isotopes still changing significantly after dolomitization (Fig. 5). During the weathering period, meteoric water intrusion led to the dissolution of gypsum to form mold pores, which also led to a $\delta^{18}O$ significant negative bias and C isotope was affected by the weathering together, showed a significant correlation. While the C isotopic characteristics of $Ma5_{3+4}$ are similar to those of the Middle Ordovician to some extent (Fig. 5) (e.g., Henderson et al., 2018), the lithology of $Ma5_{3+4}$ is mainly breccia which indicates weathering. This may be mainly because of the coupling of sedimentary environment and weathering, which did not produce an obvious shift in C/O isotopic characteristics (Allan and Wiggins, 1993). The gradual increase of seawater salinity during the Sabkha environment generally led to a significantly positive C isotopic composition, while the later meteoric water resulted in a negative C isotope deviation, which was similar to the contemporaneous seawater value.

In the Sabkha dolomitization mode, Mg is provided by diffusion, the dolomitization fluid is directly derived from the contemporaneous seawater which is affected by the evaporitic tidal flat environment. This process can be simulated by the diffusion-advection-reaction model (DAR) (Huang K. et al., 2015; Peng et al., 2016; Ning et al., 2020), which results in a downward increasing $\delta^{26}Mg_{dol}$ profile (Fig. 10a) (Geske et al., 2015a; Huang K. et al., 2015; Ning et al., 2020). However, theoretical change is significantly different from the measured Mg isotope (Fig. 3, Table 1); the reason may be similar to that of the C and O isotopes, all of which are caused by the influence of weathering during the later period.

### 5.1.2. *Brine-reflux dolomitization mode*

Petrological and geochemical characteristics show that RD3 was formed by the brine-reflux dolomitization mode (Figs. 3 and 9) (Allan and Wiggins, 1993; Warren, 2000). Stratigraphic lithology is dominated by limestone in the lower part and dolomite in the upper part nowadays, which indicates the dolomitization fluid flowed through the upper stratum (Fig. 3; Fig. 10b). The dolomite matrix of the silty crystalline indicates that dolomitization occurred in a relatively low temperature environment. In addition, the matrix dolomite has low Fe, MnO, and Sr (Table 2), showing that the dolomitized fluid cannot be deep hydrothermal (Zhao et al., 2005; Jiang et al., 2019). Dolomitization fluid of $Ma5_5$, therefore, was derived from the high salinity brine in the overlying Sabkha environment with brine-reflux (Warren, 2000; Sun, 2020). The high-

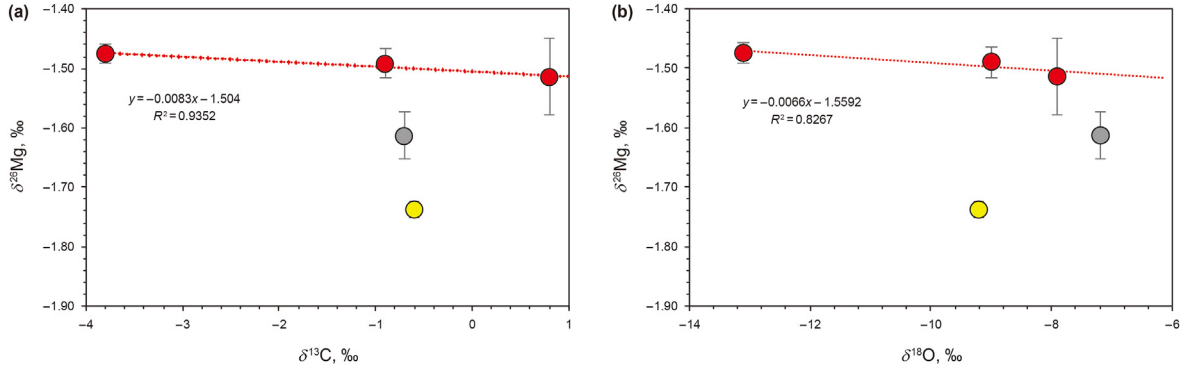


**Fig. 8.** The relationship between Mg isotope and (a) C, (b) O isotope, which were significantly correlated in $Ma5_{1+2}$ (The legend is shown in Fig. 5). The red dotted line is a good correlation between Mg isotope and C/O isotopes of $Ma5_{1+2}$.

**Table 2**
Element compositions of dolomite near weathering crust in the Daniudi area of the Ordos Basin.

| Sample | Depth, m | Major element compositions, % | | | | | | | | Trace element compositions, μg/g | | | | |
|---|---|---|---|---|---|---|---|---|---|---|---|---|---|---|
| | | MgO | CaO | MnO | Na | Fe | Al | Si | Ti | Hf | Nb | Ta | Zr | Sr |
| D113–1 | 2948.03 | 20.49 | 30.54 | 0.01 | 0.02 | 0.18 | 0.17 | 3.15 | 0.007 | 0.068 | 0.131 | 0.010 | 2.340 | 71.100 |
| D113–13 | 2911.90 | 20.47 | 30.87 | 0.01 | 0.02 | 0.38 | 0.19 | 2.11 | 0.008 | 0.059 | 0.169 | 0.014 | 1.690 | 85.300 |
| D113–21 | 2888.75 | 17.06 | 34.58 | 0.01 | 0.04 | 0.83 | 0.12 | 1.42 | 0.006 | 0.048 | 0.160 | 0.014 | 1.660 | 77.100 |
| D113–25 | 2861.71 | 21.20 | 29.70 | 0.04 | 0.02 | 2.29 | 0.10 | 0.16 | 0.009 | 0.064 | 0.245 | 0.018 | 2.190 | 49.500 |
| D113–28 | 2860.30 | 17.56 | 33.43 | 0.05 | 0.01 | 2.69 | 0.13 | 0.29 | 0.010 | 0.051 | 0.198 | 0.013 | 1.640 | 61.600 |
| D113–29 | 2854.04 | 22.27 | 29.76 | 0.01 | 0.02 | 0.34 | 0.09 | 0.29 | 0.009 | 0.032 | 0.151 | 0.010 | 1.210 | 73.900 |

**Table 3**
X-ray diffraction results of whole rock near weathering crust in the Daniudi area of the Ordos Basin.

| Samples | Depth, m | Quartz, wt% | K-feldspar, wt% | Calcite, wt% | Dolomite, wt% | Total |
|---|---|---|---|---|---|---|
| D113–1 | 2948.03 | 4.3 | / | 4.4 | 91.3 | 100.0 |
| D113–13 | 2911.90 | 2.3 | / | 16.4 | 81.3 | 100.0 |
| D113–21 | 2888.75 | 2.5 | / | 17.3 | 80.1 | 99.9 |
| D113–25 | 2861.71 | / | / | / | 98.0 | 98.0 |
| D113–28 | 2860.30 | / | / | 13.4 | 86.6 | 100.0 |

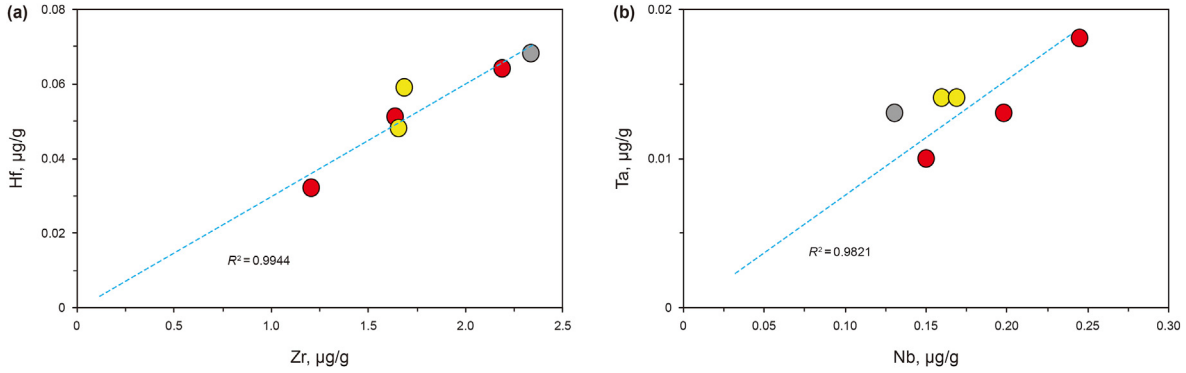


**Fig. 9.** Scatter plot of Zr–Hf, and Nb–Ta. The relationship between trace elements and weathering (The legend is shown in Fig. 5). The blue dotted line represents the weathering degree of the Ma5 Member.

salinity brine rich in $Mg^{2+}$ migrated from the upper to lower part, then the upper calcite or aragonite was dolomitized first.

The $\delta^{13}C$ measured in $Ma5_5$ is consistent with the Middle Darriwilian (Yang et al., 2022), proving this formation was relatively less affected by later diagenesis, and no correlation between C and O isotopes exists, therefore, the geochemical signals of the stratigraphy should be well preserved (Fig. 5).

In the brine-reflux dolomitization mode which can be explained by the advective flow model (AF) (Peng et al., 2016), light Mg isotope tends to enter the aragonite or calcite first to undergo metasomatism. With the development of dolomitization, heavy Mg isotope in fluid gradually enriches and leads to a higher $\delta^{26}Mg$ content of late precipitation dolomite, which is the reason why the $\delta^{26}Mg_{dol}$ increases downward in the brine-reflux dolomitization mode (Peng et al., 2016; Ning et al., 2020). The trend is consistent with the data we obtained (Fig. 3; Fig. 10b).

### 5.2. Influence of lithology on weathering

Trace elements in the $Ma5_{1-5}$ basically fall on the same weathering trend (Fig. 9), indicating that these five layers have a strong genetic connection, and the influence of other substances is relatively weak (Ling et al., 2019). In the stratum rich in gypsum ($Ma5_{1+2}$ and $Ma5_{3+4}$), this part was affected by weathering, but the influence of weathering in different formations was also different (Fig. 4).

During the period of uplift, the $Ma5_{1+2}$ were above the highest phreatic level and located in the vertical vadose zone (Bai et al., 2002). The identification of the vertical seepage zone based on the presence of near vertical solution fractures (Fig. 4a and b), aluminous mudstone migrated downward to the matrix (Fig. 4b) (He et al., 2013). Dissolution was severely affected by weathering which occurred in gypsum-bearing dolomite, although a certain amount of cement was filled in partial dissolution pores during a later stage, various dissolved pores were still left (Fig. 4g and h).

The $Ma5_{3+4}$ developed below the highest phreatic surface and is located in the horizontal underflow zone, the fluids mainly flowed in the horizontal direction (Bai et al., 2002). The main characteristics of the horizontal underflow zone are network or near horizontal dissolution fractures (Fig. 4d) and breccia (Fig. 4e) formed by weathering (He et al., 2013). Gypsum was the main dissolution target, then the dissolution strength of the matrix was weaker than that of the vertical vadose zone. The trace of gypsum cannot be observed under the microscope after weathering, some pores were filled with secondary calcite (Fig. 4i), and/or the stratum collapsed to form breccia (Fig. 4j). And fluid migrated to the lower strata after weathering the $Ma5_{1+2}$ strata which salinity content is high. When entering the horizontal underflow zone, the fluid was oversaturated with $Ca^{+}$, and calcite was prone to precipitation (Fig. 4i).

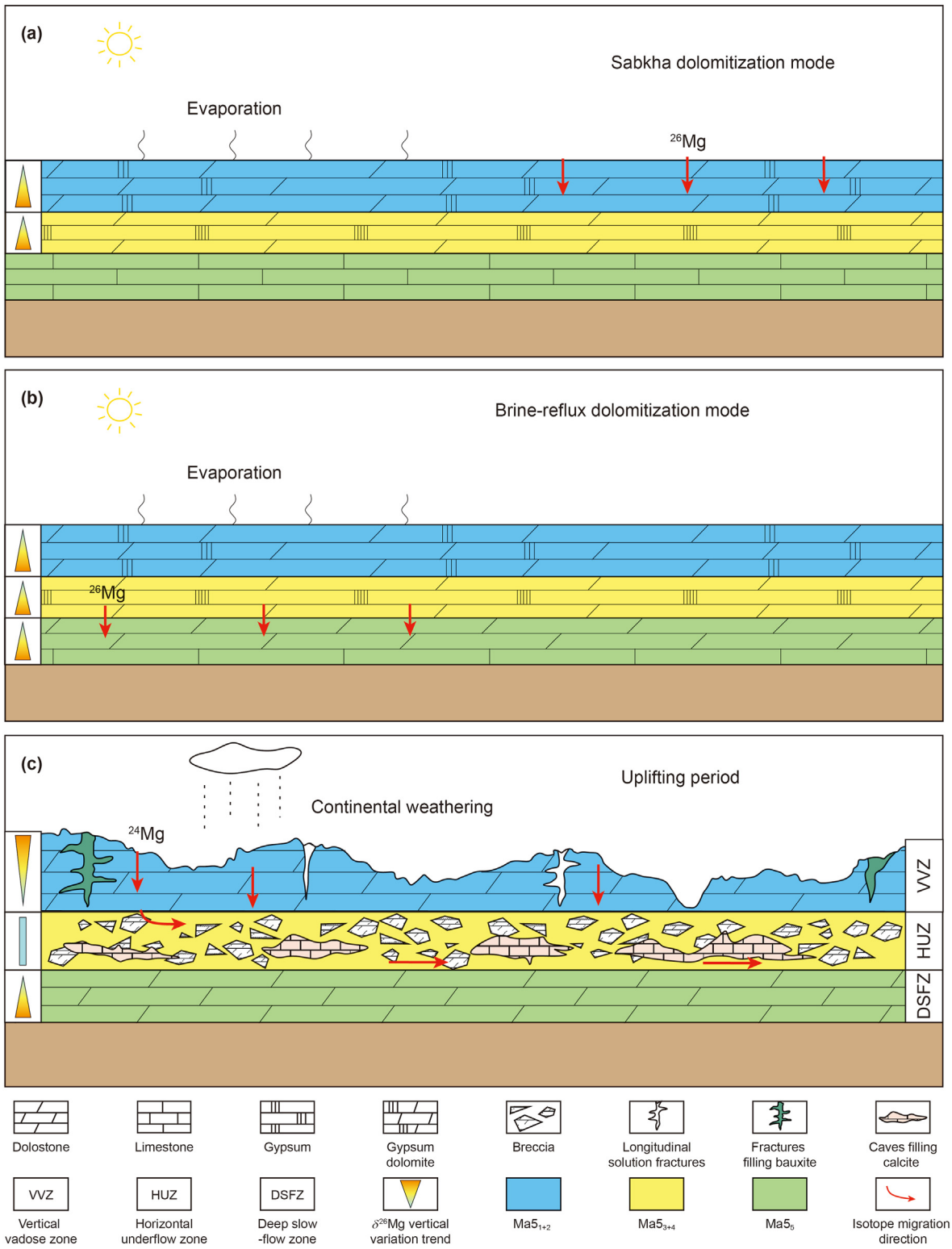


**Fig. 10.** Process of Mg isotope variation from the dolomitization modes to weathering.

In comparison, the $Ma5_5$ was weakly affected by weathering. The stratum was located in the deep slow-flow zone, and the lithology was pure dolomite and limestone (Figs. 3, 4k–l), which was easier to preserve the original isotopic characteristic than the upper strata (Figs. 3 and 5).

### 5.3. Fractionation of Mg isotope of ancient dolomite in karst crust

In the vertical seepage zone, the $\delta^{26}Mg_{dol}$ showed a downward decrease that was only controlled by weathering. And the weathering intensity was limited by the distance from the unconformity when the weathering was strong enough. The original mineral

composition has been modified by weathering, resulting in the fractionation of Mg isotope during the original dolomitization was impossible to be observed.

Dolomite was formed by the Sabkha dolomitization mode during the vertical vadose zone; however, the $\delta^{26}Mg_{dol}$ trend is contrary to the result of the DAR simulation. Both C/O isotopes and Mg isotope show strong fractionation with the increase in weathering degree, and their negative coupling changes may have a certain indication of strong weathering (Fig. 8) (Pokrovsky et al., 2011). Therefore, the fractionation of the Mg isotope is similar to that of C and O isotopes and is affected by weathering. The stratum closest to the unconformity is affected by the strongest weathering. The characteristics of vertical seepage can be seen on the core (Fig. 4a–c), and the C and O isotopes show a strong correlation which is a direct display of weathering (Fig. 5). In conclusion, this part of $\delta^{26}Mg_{dol}$ is unlikely to be the result of original dolomitization, which finally appears to be the opposite of DAR simulation. Meanwhile, the intensity of weathering was not static. Here we can judge the intensity of weathering according to the distance between the stratum and the weathered surface because the weathering in the study area had a genetic relationship (Fig. 9) (Gao et al., 2016). The $\delta^{26}Mg_{dol}$ changed to a certain extent with the intensity of weathering, which was mainly manifested as a downward decrease. This phenomenon is related to the difference in Mg isotopes between insoluble silica and carbonate component. As weathering progresses, the carbonate component is more prone to weathered, and the silica component gradually enriches until only the silica component that cannot be weathered remains (Tipper et al., 2012; Gao et al., 2016). The test results show the content of $\delta^{26}Mg$ in the insoluble silica component (−0.6‰ to +0.6‰) is significantly higher than that of the carbonate component (−1.8‰ to −1.4‰) (Table 1).

In the horizontal underflow zone, the reason for the fractionation of the $\delta^{26}Mg_{dol}$ might be (1) secondary calcite precipitation mixes with matrix, fractionation between matrix dolomite and formation fluid rich in light Mg isotope are the reasons for the negative bias of the $\delta^{26}Mg_{dol}$; (2) transverse fluid is the key to the trend of the $\delta^{26}Mg_{dol}$ changes is not obvious in the vertical direction. Finally leads to the unchanged downward and negative bias trend.

Weathering is an important reason that affects the $\delta^{26}Mg_{dol}$ in the horizontal underflow zone. However, the dissolution of matrix dolomite caused by weathering was weaker than that of the overlying strata due to the different contents of gypsum. The dissolution of gypsum produced $Ca^{+}$, and a large amount of secondary calcite was precipitated nearby (Fig. 4i). The $\delta^{26}Mg$ in secondary calcite cement is more negative than that in dolomite (Gao et al., 2016). Therefore, the $\delta^{26}Mg_{dol}$ which was mixed with various secondary calcite was significantly negative compared to other formations. In addition, the fluid that weathered $Ma5_{1+2}$ was rich in light Mg isotope. After this part of the fluid entered $Ma5_{3+4}$, strong fractionation between fluid and matrix dolomite was possible, which led to a negative deviation of $\delta^{26}Mg_{dol}$. Finally, since the fluid in the formations mainly showed horizontal migration, the influence of water-rock interaction was mainly shown in the horizontal change, and the vertical influence of $\delta^{26}Mg_{dol}$ was weak (Fig. 3).

In the deep slow-flow zone, this layer was weakly affected by weathering; this result can be confirmed by C/O isotopes data (Fig. 5). The Mg isotope signal therefore represents the result of fractionation during the original dolomitization period.

The dolomitized fluid migrated down to the sediments, resulting in a continuous process of precipitation and dolomitization of pre-existing calcite. When the high-salinity Mg-rich fluid penetrated into the limestone formation, the dolomite was precipitated in the form of pore filling or direct metasomatism or mixing with normal underground fluid before causing dolomitization, forming a larger-scale dolomite layer (Warren, 2000). Finally, the $\delta^{26}Mg_{dol}$ gradually increases, here $\delta^{26}Mg_{dol}$ shows an overall downward increase process (Fig. 10c) (He R. et al., 2020).

## 6. Conclusions

(1) Three types of dolomite were developed in the study area. Affected by the environment and sea-level, Sabkha and brine-reflux are the main dolomitization modes. In the Sabkha mode, dolomitized fluid came from the contemporaneous seawater, micritic dolomite and gypsum were developed together; in the brine-reflux mode, dolomitized fluid came from the overlying strata, silty crystalline dolomite and limestone were their lithological characteristics.

(2) In the ancient dolomite karst crust, the responses of geochemical characteristics in different layers to weathering are different. In the vertical vadose zone, the geochemical signals only showed the fractionation caused by the weathering intensity, decreasing with distance from the unconformity; in the horizontal underflow zone, the horizontal migration of fluid caused little longitudinal change of $\delta^{26}Mg_{dol}$, and C/O isotopic signals were not changed due to the coupling of various factors; the deep slow-flow zone was not sensitive to the influence of weathering, and retained the geochemical signals of the original dolomitization.

(3) Various factors control the different trends of $\delta^{26}Mg_{dol}$ in the ancient karst crust. In the vertical vadose zone, the main control of Mg isotope fractionation is weathering. The $\delta^{26}Mg_{dol}$ gradually enriched with the increase of weathering intensity, and finally showed a downward decrease profile. In the horizontal underflow zone, fluids and late diagenesis jointly control the fractionation of $\delta^{26}Mg_{dol}$, then showed unchanged downward and obviously negative. In the deep slow-flow zone is not restricted by later diagenesis, dolomitization occurred preferentially with light Mg isotope, resulting in heavier dolomitization fluid later, which led to the increase downward of $\delta^{26}Mg_{dol}$.

## Declaration of competing interest

The authors declare that they have no known competing financial interests or personal relationships that could have appeared to influence the work reported in this paper.

## Acknowledgements

This study was financially supported by the National Natural Science Foundation of China (42072177), National Natural Science Foundation of China (U19B6003), and Frontier Project of Chinese Academy of Sciences (XDA14010201).

## References

Allan, J.R., Wiggins, W.D., 1993. Dolomite Reservoirs: Geochemical Techniques for Evaluating Origin and Distribution. American Association of Petroleum Geologists, 9781629810966.

Azmy, K., Lavoie, D., Wang, Z.R., et al., 2013. Magnesium–isotope and REE compositions of Lower Ordovician carbonates from eastern Laurentia: implications for the origin of dolomites and limestones. Chem. Geol. 356, 64–75. https://doi.org/10.1016/j.chemgeo.2013.07.015.

Bai, W.H., Lv, X.M., Li, X.J., et al., 2002. The mode of palaeokarstification and the fine reconstruction of the palaeogeomorphology in the karst basin: taking Ordovician karst in eastern Ordos Basin for example. Geoscience 16 (3), 292–298. https://doi.org/10.3969/j.issn.1000-8527.2002.03.013 (in Chinese).

Blattler, C.L., Miller, N.R., Higgins, J.A., 2015. Mg and Ca isotope signatures of authigenic dolomite in siliceous deep–sea sediments. Earth Planet. Sci. 419,

32–42. https://doi.org/10.1016/j.epsl.2015.03.006.
Bialik, O.M., Wang, X., Zhao, S., et al., 2018. Mg isotope response to dolomitization in hinterland–attached carbonate platforms: outlook of $\delta^{26}$Mg as a tracer of basin restriction and seawater Mg/Ca ratio. Geochem. Cosmochim. Acta 235, 189–207. https://doi.org/10.1016/j.gca.2018.05.024.
Bourdon, B., Tipper, E.T., Fitoussi, C., et al., 2010. Chondritic Mg isotope composition of the Earth. Geochem. Cosmochim. Acta 74, 5069–5083. https://doi.org/10.1016/j.gca.2010.06.008.
Chakrabarti, R., Jacobsen, S.B., 2010. The isotopic composition of magnesium in the inner Solar System. Earth Planet. Sci. 293, 349–358. https://doi.org/10.1016/j.epsl.2010.03.001.
Chen, X.Y., Teng, F.Z., Huang, K.J., et al., 2020. Intensified chemical weathering during Early Triassic revealed by magnesium isotopes. Geochem. Cosmochim. Acta 287, 263–276. https://doi.org/10.1016/j.gca.2020.02.035.
Dessert, C., Lajeunesse, E., Lloret, E., et al., 2015. Controls on chemical weathering on a mountainous volcanic tropical island: Guadeloupe (French West Indies). Geochem. Cosmochim. Acta 171, 216–237. https://doi.org/10.1016/j.gca.2015.09.009.
Foster, G.L., Pogge von Strandmann, P.A.E., Rae, J.W.B., 2010. Boron and magnesium isotopic composition of seawater. Geochem. Geophys. Geosyst. 11 (8), Q08015. https://doi.org/10.1029/2010GC003201.
Galy, A., France–Lanord, C., 2001. Higher erosion rates in the Himalaya: geochemical constraints on riverine fluxes. Geology 29 (1), 23–26. https://doi.org/10.1130/0091-7613(2001)029<0023:HERITH>2.0.CO;2.
Galy, A., Bar–Matthews, M., Halicz, L., et al., 2002. Mg isotopic composition of carbonate: insight from speleothem formation. Earth Planet. Sci. 201 (1), 105–115. https://doi.org/10.1016/S0012-821X(02)00675-1.
Gao, P., Liu, G., Jia, C., et al., 2015. Evaluating rare earth elements as a proxy for oil–source correlation. A case study from Aer Sag, Erlian Basin, northern China. Org. Geochem. 87, 35–54. https://doi.org/10.1016/j.orggeochem.2015.07.004.
Gao, T., Ke, S., Teng, F., et al., 2016. Magnesium isotope fractionation during dolostone weathering. Chem. Geol. 445, 14–23. https://doi.org/10.1016/j.chemgeo.2016.07.012.
Geske, A., Lokier, S., Dietzel, M., et al., 2015a. Magnesium isotope composition of sabkha porewater and related (Sub–) recent stoichiometric dolomites, Abu Dhabi (UAE). Chem. Geol. 393–394, 112–124. https://doi.org/10.1016/j.chemgeo.2014.11.020.
Geske, A., Goldstein, R.H., Mavromatis, V., et al., 2015b. The magnesium isotope ($\delta^{26}$Mg) signature of dolomites. Geochem. Cosmochim. Acta 149, 131–151. https://doi.org/10.1016/j.gca.2014.11.003.
Guo, B., Zhu, X., Dong, A., et al., 2019. Mg isotopic systematics and geochemical applications: a critical review. J. Asian Earth Sci. 176, 368–385. https://doi.org/10.1016/j.jseaes.2019.03.001.
He, J., Fang, S., Hou, F., et al., 2013. Vertical zonation of weathered crust ancient karst and the reservoir evaluation and prediction—a case study of $M_5^5$–$M_5^1$ sub–members of Majiagou Formation in gas fields, central Ordos Basin, NW China. Petrol. Explor. Dev. 40 (5), 534–542. https://doi.org/10.1016/S1876-3804(13)60075-0.
He, R., Ning, M., Huang, K., et al., 2020. Mg isotopic systematics during early diagenetic aragonite–calcite transition: insights from the Key Largo Limestone. Chem. Geol. 558, 119876. https://doi.org/10.1016/j.chemgeo.2020.119876.
He, Z., Ma, Y., Zhang, J., et al., 2020. Distribution, genetic mechanism and control factors of dolomite and dolomite reservoirs in China. Oil Gas Geol. 41 (1), 1–14. https://doi.org/10.11743/ogg20200101 (in Chinese).
Henderson, M.A., Serra, F., Feltes, N.A., et al., 2018. Paired isotope records of carbonate and organic matter from the Middle Ordovician of Argentina: Intra-basinal variation and effects of the marine chemocline. Palaeogeogr. Palaeoclimatol. Palaeoecol. 490, 107–130. https://doi.org/10.1016/j.palaeo.2017.10.018.
Higgins, J.A., Schrag, D.P., 2010. Constraining magnesium cycling in marine sediments using magnesium isotopes. Geochem. Cosmochim. Acta 74 (17), 5039–5053. https://doi.org/10.1016/j.gca.2010.05.019.
Hu, Y., Teng, F.Z., Zhang, H.F., et al., 2016. Metasomatism–induced mantle magnesium isotopic heterogeneity: evidence from pyroxenites. Geochem. Cosmochim. Acta 185, 88–111. https://doi.org/10.1016/j.gca.2015.11.001.
Hu, Y., Teng, F., Plank, T., et al., 2017. Magnesium isotopic composition of subducting marine sediments. Chem. Geol. 466, 15–31. https://doi.org/10.1016/j.chemgeo.2017.06.010.
Huang, J., Li, S.G., Xiao, Y., et al., 2015. Origin of low $\delta^{26}$Mg Cenozoic basalts from South China Block and their geodynamic implications. Geochem. Cosmochim. Acta 164, 298–317. https://doi.org/10.1016/j.gca.2015.04.054.
Huang, K., Shen, B., Lang, X., et al., 2015. Magnesium isotopic compositions of the Mesoproterozoic dolostones: implications for Mg isotopic systematics of marine carbonates. Geochem. Cosmochim. Acta 164, 333–351. https://doi.org/10.1016/j.gca.2015.05.002.
Immenhauser, A., Buhl, D., Richter, D., et al., 2010. Magnesium–isotope fractionation during low-Mg calcite precipitation in a limestone cave – Field study and experiments. Geochem. Cosmochim. Acta 74 (15), 4346–4364. https://doi.org/10.1016/j.gca.2010.05.006.
Jia, H.C., Ding, X.Q., 2016. Characteristics of dolomite karst reservoirs in the M $5_{1+2}$ member of Majiagou Formation, Daniudi gasfield, Ordos Basin, China. J. Chengdu Univ. Technol. (Sci. Technol. Ed.) 43 (4), 415–422. https://doi.org/10.3969/j.issn.1671-9727.2016.04.04 (in Chinese).
Jiang, S., Zhang, Y., Huang, W., et al., 2019. Geochemical characteristics of Ordovician strontium isotope in the Ordos Basin. Acta Geol. Sin. 93 (11), 2889–2903. https://doi.org/10.19762/j.cnki.dizhixuebao.2019196 (in Chinese).
Kasemann, S.A., Pogge von Strandmann, P.A.E., Prave, A.R., et al., 2014. Continental weathering following a Cryogenian glaciation: evidence from calcium and magnesium isotopes. Earth Planet. Sci. 396, 66–77. https://doi.org/10.1016/j.epsl.2014.03.048.
Ke, S., Liu, S.A., Li, W.Y., et al., 2011. Advances and application in magnesium isotope geochemistry. Acta Petrol. Sin. 27 (2), 383–397 (in Chinese).
Ke, S., Teng, F.Z., Li, S., et al., 2016. Mg, Sr and O isotope geochemistry of syenites from northwest Xinjiang, China: tracing carbonate recycling during Tethyan oceanic subduction. Chem. Geol. 437, 109–119. https://doi.org/10.1016/j.chemgeo.2016.05.002.
Lash, G.G., 2018. Significance of stable carbon isotope trends in carbonate concretions formed in association with anaerobic oxidation of methane (AOM), Middle and Upper Devonian shale succession, western New York State, USA. Mar. Petrol. Geol. 91, 470–479. https://doi.org/10.1016/j.marpetgeo.2018.01.032.
Lavoie, D., Jackson, S., Girard, I., 2014. Magnesium isotopes in high–temperature saddle dolomite cements in the lower Paleozoic of Canada. Sediment. Geol. 305, 58–68. https://doi.org/10.1016/j.sedgeo.2014.03.002.
Li, J., Hao, C., Wang, Z., et al., 2020. Continental weathering intensity during the termination of the Marinoan Snowball Earth: Mg isotope evidence from the basal Doushantuo cap carbonate in South China. Palaeogeogr. Palaeoclimatol. Palaeoecol. 552, 109774. https://doi.org/10.1016/j.palaeo.2020.109774.
Li, W.Q., Beard, B.L., Li, C., et al., 2015. Experimental calibration of Mg isotope fractionation between dolomite and aqueous solution and its geological implications. Geochem. Cosmochim. Acta 157, 164–181. https://doi.org/10.1016/j.gca.2015.02.024.
Li, W.Y., Teng, F.Z., Ke, S., et al., 2010. Heterogeneous magnesium isotopic composition of the upper continental crust. Geochem. Cosmochim. Acta 74 (23), 6867–6884. https://doi.org/10.1016/j.gca.2010.08.030.
Ling, M.X., Sedaghatpour, F., Teng, F.Z., et al., 2011. Homogenous magnesium isotopic composition of seawater: an excellent geostandard for Mg isotope analysis. Rapid Commun. Mass Spectrom. 25 (19), 2828–2836. https://doi.org/10.1002/rcm.5172.
Ling, K.Y., Wen, H.J., Zhang, Z.W., et al., 2019. Geochemical characteristics of dolomite weathering profiles and revelations to enrichment mechanism of trace elements in the Jiujialu Formation, central Guizhou Province. Acta Petrol. Sin. 35 (11), 3385–3397. https://doi.org/10.18654/1000-0569/2019.11.08 (in Chinese).
Ma, L., Teng, F.Z., Jin, L., et al., 2015. Magnesium isotope fractionation during shale weathering in the Shale Hills Critical Zone Observatory: accumulation of light Mg isotopes in soils by clay mineral transformation. Chem. Geol. 397, 37–50. https://doi.org/10.1016/j.chemgeo.2015.01.010.
Mavromatis, V., Meister, P., Oelkers, E.H., 2014. Using stable Mg isotopes to distinguish dolomite formation mechanisms: a case study from the Peru Margin. Chem. Geol. 385, 84–91. https://doi.org/10.1016/j.chemgeo.2014.07.019.
Ning, M., Lang, X., Huang, K., et al., 2020. Towards understanding the origin of massive dolostones. Earth Planet. Sci. 545, 116403. https://doi.org/10.1016/j.epsl.2020.116403.
Oskierski, H., Beinlich, A., Mavromatis, V., et al., 2019. Mg isotope fractionation during continental weathering and low temperature carbonation of ultramafic rocks. Geochem. Cosmochim. Acta 262, 60–77. https://doi.org/10.1016/j.gca.2019.07.019.
Peng, Y., Shen, B., Lang, X.G., et al., 2016. Constraining dolomitization by Mg isotopes: a case study from partially dolomitized limestones of the Middle Cambrian Xuzhuang Formation, North China. G-cubed 17 (3), 1109–1129. https://doi.org/10.1002/2015GC006057.
Pogge von Strandmann, P.A.E., Elliott, E., Marschall, H.R., et al., 2011. Variations of Li and Mg isotope ratios in bulk chondrites and mantle xenoliths. Geochem. Cosmochim. Acta 75 (18), 5247–5268. https://doi.org/10.1016/j.gca.2011.06.026.
Pokrovsky, B.G., Mavromatis, V., Pokrovsky, O.S., 2011. Co–variation of Mg and C isotopes in late Precambrian carbonates of the Siberian Platform: a new tool for tracing the change in weathering regime? Chem. Geol. 290, 67–74. https://doi.org/10.1016/j.chemgeo.2011.08.015.
Schiller, M., Handler, M.R., Baker, J.A., 2010. High-precision Mg isotopic systematics of bulk chondrites. Earth Planet. Sci. 297 (1–2), 165–173. https://doi.org/10.1016/j.epsl.2010.06.017.
Schott, J., Mavromatis, V., Fujii, T., et al., 2016. The control of carbonate mineral Mg isotope composition by aqueous speciation: theoretical and experimental modeling. Chem. Geol. 445, 120–134. https://doi.org/10.1016/j.chemgeo.2016.03.011.
Sedaghatpour, F., Teng, F.Z., 2016. Magnesium isotopic composition of achondrites. Geochem. Cosmochim. Acta 174, 167–179. https://doi.org/10.1016/j.gca.2015.11.016.
Shen, B., Jacobsen, B., Lee, C., et al., 2009. The Mg isotopic systematics of granitoids in continental arcs and implications for the role of chemical weathering in crust formation. P. Natl. Acad. Sci. USA 106 (49), 20652–20657. https://doi.org/10.1073/pnas.0910663106.
Sibley, D.F., Gregg, J.M., 1987. Classification of dolomite rock textures. J. Sediment. Res. 57 (6), 967–975. https://doi.org/10.1306/212F8CBA-2B24-11D7-8648000102C1865D.
Su, Z.T., Chen, H.D., Xu, F.Y., et al., 2012. REE characters of the Majiagou dolomites in Ordos Basin. J. Jilin Univ. (Earth Sci. Ed.) 42 (2), 53–61. https://doi.org/10.13278/j.cnki.jjuese.2012.s2.035 (in Chinese).
Sun, Y.J., 2020. Study on Characteristics and Main Controlling Factors of Karst Reservoir in $Ma_5^1$–$Ma_5^4$ Submember in Northeast Part, Ordos Basin. Thesis.

Northwest University, 1–141p. (in Chinese).
Teng, F.Z., Yang, W., Rudnick, R.L., et al., 2013. Heterogeneous magnesium isotopic composition of the lower crust: a xenolith perspective. Geochem. Geophys. Geosyst. 14 (9), 3844–3856. https://doi.org/10.1002/ggge.20238.
Teng, F.Z., Hu, Y., Chauvel, C., 2016. Magnesium isotope geochemistry in arc volcanism. P. Natl. Acad. Sci. USA. 113 (26), 7082–7087. https://doi.org/10.1073/pnas.1518456113.
Tipper, E.T., Galy, A., Gaillardet, J., et al., 2006. The magnesium isotope budget of the modern ocean: constraints from riverine magnesium isotope ratios. Earth Planet. Sci. 250, 241–253. https://doi.org/10.1016/j.epsl.2006.07.037.
Tipper, E.T., Calmels, D., Gaillardet, J., et al., 2012. Positive correlation between Li and Mg isotope ratios in the river waters of the Mackenzie Basin challenges the interpretation of apparent isotopic fractionation during weathering. Earth Planet. Sci. 333-334, 35–45. https://doi.org/10.1016/j.epsl.2012.04.023.
Wang, Z., Hu, P., Gaetani, G., et al., 2013. Experimental calibration of Mg isotope fractionation between aragonite and seawater. Geochem. Cosmochim. Acta 102, 113–123. https://doi.org/10.1016/j.gca.2012.10.022.
Wang, S.J., Teng, F.Z., Bea, F., 2015. Magnesium isotopic systematics of metapelite in the deep crust and implications for granite petrogenesis. Geochem. Perspect. Lett. 1 (1), 75–83. https://doi.org/10.7185/geochemlet.1508.
Wang, S.J., Teng, F.Z., Scott, J., 2016. Tracing the origin of continental HIMU–like intraplate volcanism using magnesium isotope systematics. Geochem. Cosmochim. Acta 185, 78–87. https://doi.org/10.1016/j.gca.2016.01.007.
Warren, J., 2000. Dolomite: occurrence, evolution and economically important associations. Earth Sci. Rev. 52, 1–18. https://doi.org/10.1016/S0012-8252(00)00022-2.
Wimpenny, J., Burton, K.W., James, R.H., et al., 2011. The behaviour of magnesium and its isotopes during glacial weathering in an ancient shield terrain in West Greenland. Earth Planet. Sci. 304, 260–269. https://doi.org/10.1016/j.epsl.2011.02.008.
Xi, S.L., Xiong, Y., Liu, X.Y., et al., 2017. Sedimentary environment and sea level change of the subsalt interval of Member 5 of Ordovician Majiagou Formation in central Ordos Basin. J. Palaeogeogr. 19 (5), 773–790. https://doi.org/10.7605/gdlxb.2017.05.061 (in Chinese).
Xie, R.C., Zhou, W., Zhang, C., et al., 2020. Characteristics, influencing factors, and prediction of fractures in weathered crust karst reservoirs: a case study of the Ordovician Majiagou Formation in the Daniudi Gas Field, Ordos Basin, China. Geol. J. 55 (12), 7790–7806. https://doi.org/10.1002/gj.3907.
Yang, J.Q., Zhang, J.T., He, Z.L., et al., 2022. Paleoenvironment reconstruction of the Middle Ordovician thick carbonate from western Ordos Basin, China. Petrol. Sci. https://doi.org/10.1016/j.petsci.2022.08.027.
Yang, W., Teng, F.Z., Zhang, H.F., et al., 2012. Magnesium isotopic systematics of continental basalts from the North China craton: implications for tracing subducted carbonate in the mantle. Chem. Geol. 328, 185–194. https://doi.org/10.1016/j.chemgeo.2012.05.018.
Yang, X., 2011. Study on the Carbonate Reservoir Characteristics of Majiagou Formation in Daniudi Area, Ordos Basin. Thesis. Xi'an Shiyou University, 1–75p. (in Chinese).
Yu, C., Jia, Y., Ren, Z., et al., 2021. Geochemical characteristics and genesis of the Ma55 dolomite of Ordovician Majiagou Formation in Daniudi area, Ordos Basin. Mar. Origin Petrol. Geol. 26 (4), 375–383. https://doi.org/10.3969/j.issn.1672-9854.2021.04.010 (in Chinese).
Zhang, J.T., Jin, X.H., Li, S.J., et al., 2016. Types and origin of pore-fillings from the 5$^{th}$ member of the Ordovician Majiagou Formation in Ordos Basin. Oil Gas Geol. 37 (5), 684–690. https://doi.org/10.11743/ogg20160508 (in Chinese).
Zhang, J.T., He, Z.L., Yue, X.J., et al., 2017. Genesis of iron-rich dolostones in the 5$^{th}$ member of the Majiagou Formation of the Ordovician in Ordos Basin. Oil Gas Geol. 38 (4), 776–783. https://doi.org/10.11743/ogg20170414 (in Chinese).
Zhao, J.X., Chen, H.D., Zhang, J.Q., et al., 2005. Genesis of dolomite in the fifth member of Majiagou Formation in the Middle Ordos Basin. Acta Petrol. Sin. 26 (5), 38–47. https://doi.org/10.3321/j.issn:0253-2697.2005.05.008 (in Chinese).
Zhang, P.Y., Wang, Y.L., Wei, Z.F., et al., 2022. Carbon, oxygen and strontium isotopic and elemental characteristics of the Cambrian Longwangmiao Formation in South China: paleoenvironmental significance and implications for carbon isotope excursions. Gondwana Res. 106, 174–190. https://doi.org/10.1016/j.gr.2022.01.008.
Zhao, Y.Y., Jiang, S.Y., Li, D., et al., 2016. A petrographic and geochemical study of carbonate and silica phases from the Ediacaran Doushantuo Formation in the Three Gorges area of South China: implications for diagenetic conditions. Palaeogeogr. Palaeoclimatol. Palaeoecol. 463, 150–167. https://doi.org/10.1016/j.palaeo.2016.10.004.